Online Debonding Detection in Honeycomb Sandwich Structures Using Multi-Frequency Guided Waves

F. Song[a], G. L. Huang*[,a,b], G. K. Hu[c]
[a] Dept. of Applied Science, Univ. of Arkansas at Little Rock, Little Rock, AR, USA, 72204;
[b] Dept. of Systems Engineering, Univ. of Arkansas at Little Rock, Little Rock, AR, USA, 72204;
[c] Sch. of Aerospace Engineering, Beijing Inst. of Technol., Beijing, China, 100081

ABSTRACT

Due to the complex nature of sandwich structures, development of the online structural health monitoring system to detect damages in honeycomb sandwich panels inherently imposes many challenges. In this study, the leaky guided wave propagation in the honeycomb sandwich structures generated by piezoelectric wafer actuators/sensors is first simulated numerically based on the finite element method (FEM). In the numerical model, the real geometry of the honeycomb core is considered. To accurately detect debonding in the honeycomb sandwich structures, signal processing based on continuous wavelet transform is adopted to filter out the unwanted noise in the leaky Lamb wave signals collected from the experimental testing. A correlation analysis between the benchmark signals at the normal condition and those recorded at the debonded condition is then performed to determine the differential features due to the presence of debonding. Finally, the image of the debonding is formed by using a probability analysis. Specifically, fusing images acquired from multi-frequency leaky Lamb waves are obtained to enhance the quality of the final image of the structure. The location and size of the debonding in the honeycomb sandwich structures are estimated quantitatively.

Keywords: Lamb waves, debonding detection, honeycomb sandwich, image fusion

1. INTRODUCTION

Due to the attractive characteristics such as high strength/stiffness-to-weight ratios and effective acoustic insulation, honeycomb sandwich structures have extensively served marine, aerospace and aeronautic industries. However, an intensive load or repeating loading in the core tends to induce debondings at the skin-core interface threatening the integrity and safety of the whole structures [1-3]. Conventional inspection approaches such as C-scan and X-ray are limited to a point-by-point manner and are quite time consuming. Therefore, the development of an online monitoring system of composite structures becomes an urgent issue and attracts a lot of attention recently. Compared with the conventional nondestructive evaluation (NDE) techniques, the online structural health monitoring (SHM) techniques can instantaneously provide reliable and quantitative structural health data for in-service composite structures, and cover a relatively large inspection area.

Ultrasonic guided wave (GW) based SHM techniques using specific transducers/receivers have shown great potential for delamination characterization in laminated composites [4]. Based on piezoelectric actuators/sensors, Su et al. [5, 6] utilized the time of flight (TOF) between the incipient fundamental symmetric Lame waves and delamination-induced fundamental shear horizontal mode to triangulate the delaminations in composite laminates. Using modally selective Lamb wave transducers, Petculescu et al. [7] demonstrated that the accumulated time delay of modal group velocity is a reliable damage parameter for quantitative monitoring of delaminations for quasi-isotropic woven and cross-ply composites. Wang and Yuan [8] performed prestack reverse-time migration technique to image the delaminations in composite laminates with a linear piezoelectric ceramic (PZT) disk array, and both the location and size of the delaminations were quantitatively obtained. However, the application of all these approaches has similar limitations: resulting scattered wave or wave velocity change due to the presence of the damage is required to capture information of the damages, which may not be observed in some damaged structures.

*glhuang@ualr.edu; phone 1 501 683-7522; fax 1 501 569-8698

Second International Conference on Smart Materials and Nanotechnology in Engineering,
edited by Jinsong Leng, Anand K. Asundi, Wolfgang Ecke, Proc. of SPIE Vol. 7493,
74931K · © 2009 SPIE · CCC code: 0277-786X/09/$18 · doi: 10.1117/12.845752

Owing to the dramatic acoustic impedance difference between the core and skin and high core-to-skin thickness ratio, the GW propagation in honeycomb sandwich structures was characterized as leaky GWs at sufficiently high frequency [9, 10]. It was found that the GW energy dissipated into the core is responsible for significant wave attenuation. Neither scattered wave nor obvious wave velocity change due to the appearance of skin-core debondings was observed experimentally [11]. To identify skin-core delamination or debonding in honeycomb sandwich structures, the leaky GW has been regarded as a potential way based on the change of the amplitude, energy or the shape of transmitted GW signals [12] in time or frequency domain. Using the leaky surface wave propagation in the honeycomb composite, Qi et al. [13] compared ultrasonic wave transmission energy between the baseline at normal conditions and the debonding specimen for the identification of the skin-core debonding. Hay et al. [14] theoretically simulated the Leaky Lamb waves in the composite skin and the sensitivity of various Lamb wave modes to the composite skin-Nomex core debonding was presented by frequency sweeping using wedge transducers, but the quantitative assessment of debonding information was not provided. Based on the frequency domain damage index approach [15], Baid et al. [16] indentified and located the composite skin-honeycomb core debond using ultrasonic sensor arrays. In the study, the localization of the skin-core debond required clusters of sensor arrangements, and the information about the damage size was completely left unknown. The systematic GW techniques for quantitative skin-core debonding detection in honeycomb sandwich structures are, however, not well documented.

To overcome those aforementioned limitations, in this study, the ultrasonic imaging approach is proposed to locate and size the skin-Nomex honeycomb core debonding based on the leaky Lamb waves by using a sparse piezoelectric wafer actuator/sensor network. In the paper, a three-dimensional finite element (FE) model, which takes into account the real geometry of regular hexagonal honeycomb core, is first used to study leaky Lamb waves in honeycomb sandwich structures. In the numerical model, the surface-bonded PZT (Piezoelectric Lead Zirconate Titanate) wafer actuators/sensors are used. An experimental testing with a sparse PZT actuator/sensor network is then conducted to generate leaky Lamb waves at different frequencies to indentify the skin-core debonding. To accurately identify debonding in the honeycomb sandwich structures, signal processing based on continuous wavelet transform is performed to filter out the measurement noise. A correlation analysis between the normal benchmark signals and those recorded at damaged conditions is conducted to determine the appropriate damage indicator. Finally, fusing images acquired from multi-frequency leaky Lamb waves are obtained to enhance the quality of the final image of the structure. The location and size of the debonding in the honeycomb sandwich structures are quantitatively estimated.

2. NUMERICAL SIMULATION OF LEAKY LAMB WAVES

Owing to the complex structural geometry and boundary conditions, it is not practical to accurately predict the GW propagation in honeycomb sandwich structures by using analytical modeling approaches. In the section, the leaky Lamb wave propagation generated by a surface-bonded PZT actuator/sensor system is briefly investigated based on three-dimensional FE models. A commercially available FE code, ANSYS/Multiphysics 11.0, is used. In the FE modeling, the SOLID5 element with eight nodes and six degree of freedoms (DOF) at each node is selected for the PZT patches to consider electromechanical coupling behavior. The additional DOF in the coupled field element is electrical voltage. Input voltage can be applied on the top nodes of the PZT actuator, and zero voltage is assigned on the bottom nodes of the PZT actuator and sensor for the simulation of grounding operation. The SOLID45 element is used to model two skin panels, and the SHELL63 element is considered to model real geometry of the hexagonal cells. The detailed FE model can be found in Ref. [10]. In the simulation, the PZT actuator-sensor distance is 172.8*mm*. The geometry parameters of the composite are shown in Table 1.

Table 1. Geometry parameters of the honeycomb sandwich structure and PZT actuators/sensors. (Units: *mm*)

Skin panels			Honeycomb core			PZT actuator/sensor	
Length	Width	Thickness	Cell size	Wall thickness	Height	Diameter	Thickness
283.2	116.4	2.0	4.8	0.22	15.0	6.35	0.76

Due to the symmetry of the problem, only a half volume of the structure is taken into account and symmetric boundary condition is applied on all the nodes on the symmetric plane. For the convergence of dynamic simulation, mesh of the

structure should be fine enough such that at least ten elements exist per wavelength along the direction of wave propagation. The integration time step should be also sufficiently small to resolve the frequency response of the structure.

The aluminum alloy T6061 and Nomex are used for skin panel and core material in the simulation, respectively. The material properties are shown in Table 2.

Table 2. Material properties of skins and honeycomb core

Material	Young's modulus (GPa)	Poisson's ratio	Density (kgm^{-3})
Aluminum alloy T6061	70	0.33	2700
Nomex	9	0.30	1384

The piezoelectric material properties are assumed as

$$[\varepsilon]=\begin{bmatrix} 6.45 & 0 & 0 \\ & 6.45 & 0 \\ & Symmetry & 5.62 \end{bmatrix}\times 10^{-9}\left(CV^{-1}m^{-1}\right), \qquad [e]=\begin{bmatrix} 0 & 0 & -5.2 \\ 0 & 0 & -5.2 \\ 0 & 0 & 15.1 \\ 0 & 0 & 0 \\ 0 & 12.7 & 0 \\ 12.7 & 0 & 0 \end{bmatrix}\left(Cm^{-2}\right)$$

and

$$[c]=\begin{bmatrix} 13.9 & 6.78 & 7.43 & 0 & 0 & 0 \\ & 13.9 & 7.43 & 0 & 0 & 0 \\ & & 11.5 & 0 & 0 & 0 \\ & & & 3.56 & 0 & 0 \\ & & & & 2.56 & 0 \\ & & Symmetry & & & 2.56 \end{bmatrix}\times 10^{10}(Pa)$$

where $[\varepsilon]$ is the dielectric matrix, $[e]$ is the piezoelectric matrix, and $[c]$ is the stiffness matrix. The density of the PZT material is assumed to be 7700 kgm^{-3}.

The GW behavior of the honeycomb sandwich structures were investigated in detail for a wide range of frequencies based on FE simulation [10]. The snapshot of the out-of-plane wave field generated by the piezoelectric actuator at the time instant $t=9.2\times10^{-5}s$ is demonstrated in Fig. 1(a) for the narrow band tone burst excitation at central frequency f_c=100kHz. It is evident that the deformation due to the GW propagation is mainly concentrated in the upper skin panel of the composite. The wave propagation mechanism at this frequency can be regarded as the leaky Lamb wave propagation in the upper plate structure. To further study leaky wave mechanism, Fig. 1(b) shows the comparison of the corresponding normalized sensor signals at the frequency f_c=100 kHz for both the lowest symmetric mode S_0 and the lowest antisymmetric mode A_0. For clear demonstration of core effects, the sensor signal from the single plate that has the same geometrical dimension and material properties as the skin panel of the honeycomb composite is collected and plotted. In the figure $Am^*=Am/Am_{max}$ is the normalized sensor amplitude with Am being the magnitude of the sensor signal and Am_{max} being the maximum value of all sensor magnitudes plotted in the figure. The results in the figure show that the sensor response predicted by the single plate is fairly consistent with the wave response of the honeycomb sandwich structure in phase, and obvious attenuation in amplitude can be clearly observed in the presence of honeycomb core, which are typically the leaky properties of Lamb waves. The leakage to the core is responsible for attenuation, which strongly depends on the ratio of in-plane and out-of-plane displacements at the interface for a given mode.

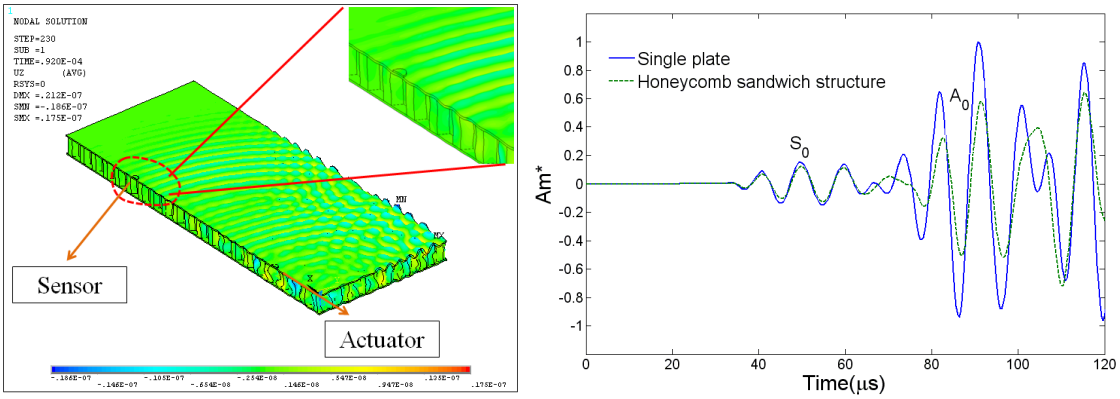

(a) (b)

Fig. 1. Simulation of wave propagation in the honeycomb sandwich structure for f_c=100 kHz. (a) The out-of-plane wave field generated by the PZT actuator; (b) The comparison of the normalized sensor responses obtained from the single plate and the honeycomb sandwich structure.

3. EXPERIMENTAL TESTING FOR HONEYCOMB SANDWICH SHM

3.1 Experimental setup

The experimental setup in this study is shown in Fig. 2(a). Both pristine and debonding honeycomb sandwich panel specimens ($609.6mm \times 609.6mm \times 19mm$) are prepared for testing, with aluminum alloy (T6061) skins and hexagonal celled Nomex core (HRH-78 honeycomb, Hexcel Corporation). A rectangular Teflon film ($30mm \times 10mm \times 0.1mm$) was inserted into the skin-core interface during the fabrication to simulate skin-core debonding. The example sensing network is composed of nine PZT patches (6.36*mm* in diameter; 0.76*mm* in thickness; APC International Ltd. 850), as shown in Fig2. (b). One of the PZT patches is used as actuator to generate ultrasonic signals and the rest are listening to form an "active" local sensing system. The spacing between two PZT patches is 127.0*mm*. The commercial cyanoacrylate adhesive is used to bond the PZT patches to the surface of the specimen. A peak-to-peak value of 10V of five-peak tone burst ultrasonic signals is generated by the function generator (Tektronix AFG3021) and applied to the PZT actuator to excite the structure. Signals from the sensors are collected by the digital oscilloscope (Tektronix DPO4034) and processed in the computer by the software Ni SignalExpress. The transient signals are digitized with 10000 points using a sampling interval of $0.04\mu s$.

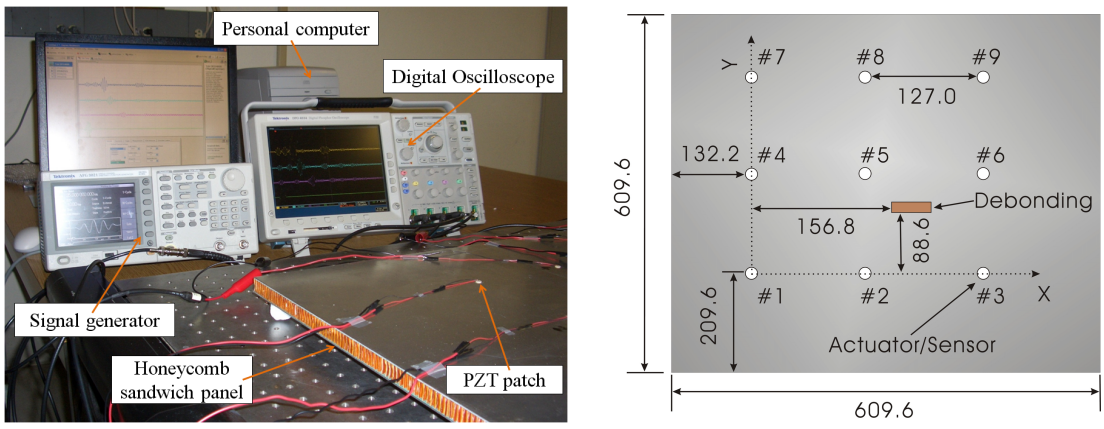

(a) (b)

Fig. 2. (a) The experimental setup of PZT patches surface-bonded to a honeycomb sandwich panel; (b) downward view of the detailed PZT actuator/sensor network arrangement (unit: *mm*).

3.2 Signal processing

Fig. 3 shows the example waveforms collected from actuator-sensor pairs #3 and #5 for excitation frequency f_c=175 kHz and f_c=375kHz with and without debonding, respectively. Based on the group velocity obtained in the composite materials, it can be found that both the S_0 mode and the A_0 mode are generated with lower excitation frequency f_c=175 kHz, while only the dominated S_0 mode is clearly seen with higher frequency f_c=375 kHz. A number of experimental observations have shown that the laminated composite delaminations lead to incipient Lamb wave attenuation, and additional scattered waves [5, 17]. However, the comparison between the benchmark sensor response and the signal received from the debonding honeycomb sandwich specimen reveals that the appearance of skin-core debonding primarily results in an observable amplitude increase in the sensor responses. It is understandable since less GW energy is leaked to the core when the GWs propagate through the debonding area. It is also interested to notice that no scattered wave group is clearly observed for both excitation frequencies. Therefore, those velocity-measurement based methods may not be suitable for skin-honeycomb core debonding detection. Compared with that at f_c=375kHz, the sensor response at f_c=175kHz has the lower signal-to-noise ratio due to small amplitude. Therefore, the signal processing is strongly recommended for multi-frequency wave signals before they are used for the damage characterization.

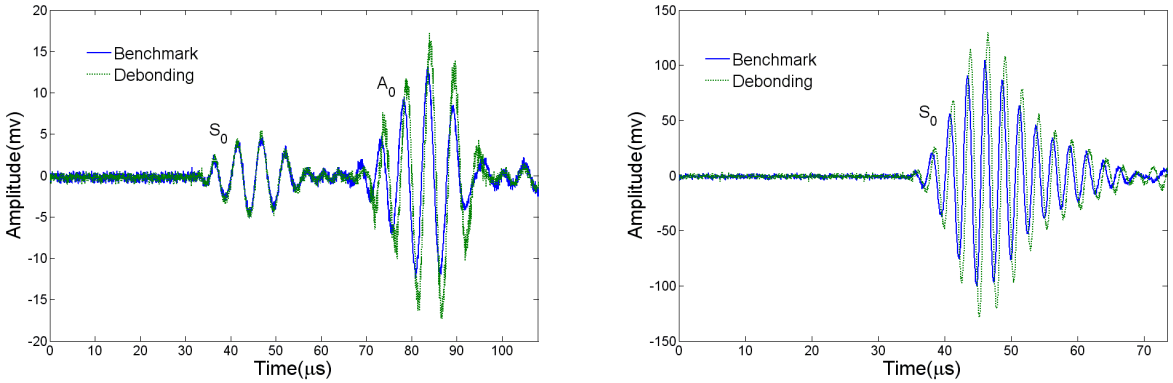

Fig. 3.Sample waveforms of the actuator-sensor pair (#3, #5) for different frequencies. (a) f_c=175 kHz; (b) f_c=375 kHz.

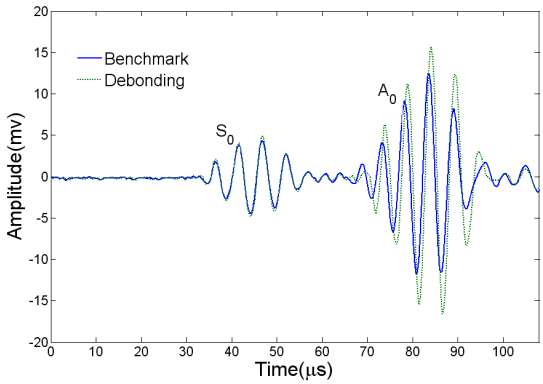

Fig. 4. Filtered results for sensor signals in Fig. 3 (a).

To minimize the measurement noise, a continuous wavelet transformation filtering is conducted. The wavelet transformation coefficients are first computed based on the sensor signals collected in the experimental testing. The filtered signals can be then reconstructed via the inverse continuous wavelet transform by restricting the integration operation to include only the part near the driving frequency (i.e. the lower and upper limits of the narrowband excitation frequency). The frequency components outside the driving frequency are then filtered out [18]. In the study, the Gabor wavelet [17, 19, 20] is selected as the mother wavelet in the wavelet transform. Fig. 4 gives the filtered sensor signals for the sensor responses in Fig. 3(a). It is evident that disturbances from other frequencies can be removed and the background noise is hence much reduced, which is beneficial for further damage characterization.

4. DEBONDING DETECTION BY USING MULTI-FREQUENCY GWS

In this section, the filtered sensor signals collected from various actuator-sensor pairs at different frequencies in the experimental testing are used for quantitative debonding characterization in honeycomb sandwich structures. The signal correlation analysis is conducted to obtain the damage differential feature. The image of the structure is obtained by using a probability analysis at individual frequency. The individual image is finally fused to enhance the imaging information about the debonding location and size.

4.1 Image generation

The signal change of the actuator-sensor pair (#*i*, #*j*) can be represented by the drop in the correlation coefficient between the signal and benchmark, which is given by [21]

$$E_{ij} = 1 - \left(M\sum_{k=1}^{M} X_k Y_k - \sum_{k=1}^{M} X_k \sum_{k=1}^{M} Y_k \right) \Bigg/ \left[\sqrt{M\sum_{k=1}^{M} X_k^2 - \left(\sum_{k=1}^{M} X_k \right)^2} \cdot \sqrt{M\sum_{k=1}^{M} Y_k^2 - \left(\sum_{k=1}^{M} Y_k \right)^2} \right] \tag{1}$$

where X is the benchmark data from the actuator-sensor pair (#*i*, # *j*) and Y is each new set of data recorded with damages, and M is the length of the data set. The motivation behind this feature is that the correlation coefficient function is affected only by changes in the shapes of the signals.

To determine the location of the debonding, the inspection area within the sensor network is discretized into a set of imaging pixels (x, y). The defect distribution probability within the sensor network can hence be expressed as a linear summation of all the signal change effects of every possible actuator-sensor pair, each of which has a spatial distribution. The simple linearly decreasing elliptical distribution is assumed in this study, with the actuator and sensor at the foci. Assuming that there are total N PZT patches within the sensor network, the estimation of the defect probability at imaging pixel (x, y) within the reconstruction region $C(x, y)$ can be described as [12]

$$C(x,y) = \sum_{i=1}^{N-1} \sum_{j=i+1}^{N} E_{ij} \left[\frac{\alpha - B_{ij}(x,y)}{\alpha - 1} \right] \tag{2}$$

where $C(x, y)$ is the defect distribution probability estimation from the actuator #*i* to sensor #*j* pair.

$$B_{ij}(x,y) = \begin{cases} D_{ij}(x,y) & D_{ij}(x,y) < \alpha \\ \alpha & D_{ij}(x,y) \geq \alpha \end{cases} \tag{3}$$

where $D_{ij} = \left[\sqrt{(x-x_i)^2 + (y-y_i)^2} + \sqrt{(x-x_j)^2 + (y-y_j)^2} \right] \Big/ d$ with d being the distance between the actuator #*i* and sensor #*j*, and α is a scaling parameter usually selected around 1.05 [12]. Note that if we consider a spatially distributed actuator/sensor network of N discrete PZT patches surface-bonded to the honeycomb sandwich panel at known locations, there are only a total of $N(N\text{-}1)/2$ actuator-sensor combinations needed due to reciprocity.

4.2 Multi-frequency image fusion

Image fusion refers to the combining, or fusing, of the multiple images to obtain an improved image; i.e. better signal-noise-ratio and more accurate localization of damage [22]. Since modes travel at different wave velocities and may interact differently with damages and geometry at different frequencies, a particular artifact may appear at different locations on the individual images, or be absent completely from some images. It is feasible to compound images to reduce artifacts and preserve damage identification. In this study, the average of all the corresponding pixels in the individual images is selected as the strategy for the fusing process [23].

Fig. 5 shows single frequency image using the sensor signals at f_c =175 kHz for 36 actuator-sensor pairs based on Eq. (2). In the image, the probability value is normalized with respect to the maximum value, and the lighter the pixel value is, the higher the chance that the debonding is located there. The white dots denote the actuator/sensor locations, and the rectangular contour describes the actual shape and location of the debonding. It is seen that although the size and location of the debonding are estimated, the presence of artifacts greatly lowers the resolution of damage diagnostic images for the current sparse sensor network.

By averaging 15 individual images from 150kHz to 375kHz, the fused image is demonstrated in Fig. 6(a). Compared with the individual image of Fig. 5, the fused images of Fig. 6 (a) clearly have fewer and lower amplitude artifacts. The improvement is attributed to the fact that the various artifacts change in location with frequency, and the main response from the debonding remains at the same location. Fig. 6(b) shows the binary image created from Fig. 6(a) by only accounting for image pixels whose intensity is bigger than an appropriate threshold value, which is chosen as 95% of the maximum intensity of the reconstructed damage localization image, where the white area denotes the estimated debonding area, and the rectangular contour gives the actual shape and location of the debonding. From Fig. 6(b), it can be observed that the estimated debonding location agrees quite well with the actual location of the simulated skin-core debonding, which demonstrates that the application of fusing damage images from the multi-frequency Lamb waves remarkably improves quality of the estimated debonding location and size.

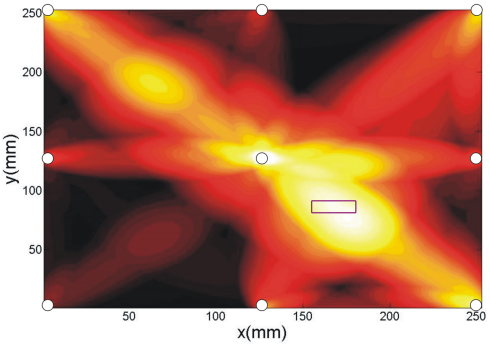

Fig. 5. Debonding image with f_c =175kHz.

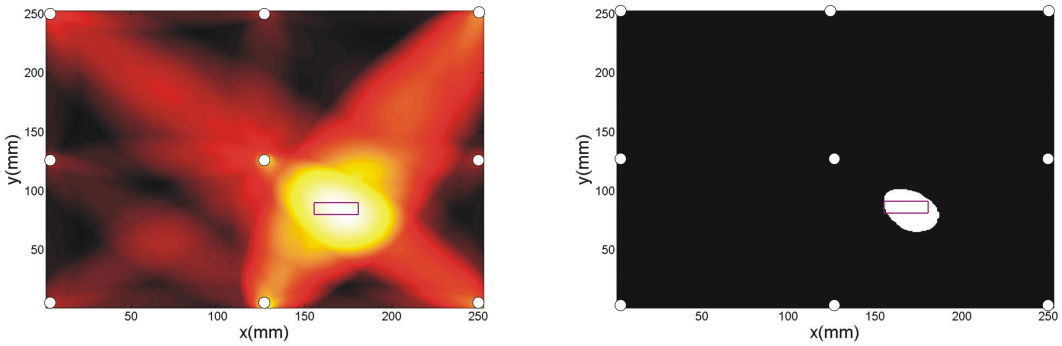

(a) (b)

Fig. 6 (a). Fused image with muti-frequency Lamb wave data; (b) the corresponding binary image.

5. SUMMARY AND CONCLUSIONS

In this study, the leaky Lamb wave propagation in the honeycomb sandwich structures generated by the piezoelectric actuators/sensors is revealed by using FE simulation. Based on the Leaky Lamb waves, the ultrasonic imaging approach with signal correlation analysis is applied to characterize the skin-core debonding, and the diagnostic image of the structure is formed by using a probability analysis of damage occurrence. It is demonstrated that the use of fusing damage images obtained from the multi-frequency Lamb waves dramatically improves image information about the estimated debonding location and size.

ACKNOWLEDGEMENTS

This research was partly supported by the National Science Foundation Grant No. EPS-0701890 and NASA EPSCoR RID grant.

REFERENCES

1. S. Goswami and W. Becker, "Analysis of debonding fracture in a sandwich plate with hexagonal core," *Compos. Struct.* 49(4), 385-392 (2000).
2. G.A.O. Davies, D. Hitchings and J. Ankersen, "Predicting delamination and debonding in modern aerospace composite structures," *Compos. Sci. Technol.* 66(6), 846-854 (2006).
3. N. Takeda, S. Minakuchi and Y. Okabe, "Smart composite sandwich structures for future aerospace application-damage detection and suppression-: A review," *J. solids Mech. Mater. Eng*. 1(1), 3-17 (2007).
4. W. J. Staszewski, S. Mahzan and R. Traynor, "Health monitoring of aerospace composite structures – Active and passive approach," *Compos. Sci. Technol.* 69(11-12), 1678-1685 (2009).
5. Z. Su, L. Ye and X. Bu, "A damage identification technique for CF/EP composite laminates using distributed piezoelectric transducers," *Compos. Struct.* 57(1-4), 465–471 (2002).
6. Z. Su, X. Wang, Z. Chen, L. Ye and D. Wang, "A *built-in* active sensor network for health monitoring of composite structures," *Smart Mater. Struct.* 15, 1939-1949 (2006).
7. G. Petculescu, S. Krishnaswamy and J. D. Achenbach, "Group delay measurements using modally selective Lamb wave transducers for detection and sizing of delaminations in composites," *Smart Mater. Struct.*17, 015007 (2008).
8. L. Wang and F. G. Yuan, "Damage identification in a composite plate using prestack reverse-time migration technique," *Structural Health Monitoring: An International Journal* 4(3), 195-211 (2005).
9. N. Bourasseau, E. Moulin, C. Delebarre and P. Bonniau, "Radome health monitoring with Lamb waves: experimental approach," *NDTE Int.* 33, 393-400 (2000).
10. F. Song, G. L. Huang and K. Hudson, "Guided wave propagation in honeycomb sandwich structures using a piezoelectric actuator/sensor system," *Smart Mater. Struct.* 18, 125007 (2009) .
11. F. C. He, Z. G. Zhou and Z. Y. Feng, "Research on an inspection method for De-bond defects in aluminum skin-honeycomb core sandwich structure with guided waves," *17 th world conf. on nondestructive testing* (2008).
12. X. L. Zhao, H. D. Gao, G. F. Zhang, B. Ayhan, F. Yan, C. Kwan and J. L. Rose, "Active health monitoring of an aircraft wing with embedded piezoelectric sensor/actuator network: I. Defect detection, localization and growth monitoring," *Smart Mater. Struct.* 16, 1208-1217 (2007).
13. X. Qi, J. L. Rose, and C. G. Xu, "Ultrasonic guided wave nondestructive testing for helicopter rotor blades," *17 th world conf. on nondestructive testing*, (2008).
14. T. R. Hay, L. Wei and J. L. Rose, "Rapid inspection of composite skin-honeycomb core structures with ultrasonic guided waves," *J. Compos. Mater.* 37(10), 929-939 (2003).
15. A. K. Mal, S. Banerjee, and F. Ricci, "An automated damage identification technique based on vibration and wave propagation data," *Phil. Trans. R. Soc. A* 365(1851), 479-491 (2007).
16. H. Baid, S. Banerjee, S. Joshi and A. Mal, "Detection of disbonds in a honeycomb composite structure using guided waves," *Proc. SPIE on Health Monitoring of Structural and biological System*, (2008).
17. K. H. Ip and Y. W. Mai, "Delamination detection in smart composite beams using Lamb waves," *Smart Mater. Struct.* 13, 544-551 (2004).
18. H. W. Park, H. Sohn, K. H. Law and C. R. Farrar, "Time reversal active sensing for health monitoring of a composite plate," *J. Sound Vibrat.* 302, 50-66 (2007).
19. F. Song, G. L. Huang, J. H. Kim and S. Haran, "On the study of surface wave propagation in concrete structures using a piezoelectric actuator/sensor system," *Smart Mater. Struct.* 17, 055024 (2008).
20. L. Wang and F. G. Yuan, "Group velocity and characteristic wave curves of Lamb waves in composites: Modeling and experiments," *Compos. Sci. Technol.* 67(7-8), 1370-1384 (2007).
21. J. Cohen, *Statistical Power Analysis for the Behavioral Sciences*, Hillsdale: Lawrence Erlbaum Associate, 1988.
22. J. E. Michaels and T. E. Michaels, "Guided wave signal processing and image fusion for *in situ* damage localization in plates," *Wave Motion* 44, 482-492 (2007).
23. K. R. Leonard and M. K. Hinders, "Lamb wave tomography of pipe-like structures," *Ultrasonics* 43, 574-583 (2005).